LETTER

Should we pose a closure problem for capacitive charging of porous electrodes?

To cite this article: A. N. Shocron and M. E. Suss 2020 *EPL* **130** 34003

A Letters Journal Exploring the Frontiers of Physics

May 2020

EPL, **130** (2020) 34003
doi: 10.1209/0295-5075/130/34003

www.epljournal.org

Should we pose a closure problem for capacitive charging of porous electrodes?

A. N. Shocron[1] and M. E. Suss[1,2(a)]

[1] *Faculty of Mechanical Engineering, Technion - Israel Institute of Technology - Haifa, Israel*
[2] *Grand Technion Energy Program, Technion - Israel Institute of Technology - Haifa, Israel*

received 21 February 2020; accepted in final form 18 May 2020
published online 3 June 2020

PACS 47.56.+r – Flows through porous media
PACS 82.47.Uv – Electrochemical capacitors; supercapacitors
PACS 47.57.jd – Electrokinetic effects

Abstract – The capacitive charging of porous electrodes is crucial to various electrochemical systems which store or harvest energy, or desalinate water. Volume averaging of the equations governing system dynamics is often employed due to a random electrode pore structure, resulting in a closure problem. The closure problem introduces significant mathematical complexity, thus it is important to understand and probe under which conditions it can be neglected. We here solve for the dynamics of capacitive charging within pores of various shapes and compare to results of volume-averaged models neglecting the closure problem. We quantify errors and determine constraints under which neglecting the closure problem is largely justified, and find pore shape has a significant impact on the associated errors.

Introduction. – A multitude of electrochemical systems leverage the capacitive charging of porous electrodes, towards applications such as energy storage, energy harvesting, or water desalination. Prominent examples include electric double layer capacitors (EDLCs), which store energy in electric double layers (EDLs) that form along electrically charged pore surfaces [1–3]. In EDLCs, electrodes are soaked in electrolyte with either an aqueous or organic solvent, with aqueous electrolytes enabling higher power density while organic electrolytes allow for maximized energy density [4,5]. Capacitive charging is also employed for energy harvesting by capacitive mixing, where the difference of potential associated with charged electrodes filled by concentrated or dilute solutions is exploited [6–8]. Another example is water treatment via capacitive deionization (CDI), in which undesired ions present in feedwater are removed via electrosorption into EDLs forming along charged surfaces [9]. In CDI, ion electrosorption can be utilized for wastewater purification [9], both brackish and sea water desalination [10], water softening [11], microfluidic sample preparation [12], ion separations [13], and organic solvent remediation [14].

The electrode material used in cells performing capacitive charging are often activated porous carbon electrodes with a random mesoscale or macroscale through-electrode pore structure. As a result, modeling the ion and charge dynamics of such cells requires accounting for spatial complexities induced by the pore structure. Several techniques exist to model such a process, including direct numerical simulations layered onto 3D random pore structures [15,16], reduced order models [17,18], and homogenization or volume averaging of the governing equations [19,20]. Volume averaging is often employed as it allows for relatively simple implementation and is generally less intensive numerically. For CDI cells, a volume-averaged model was first developed by Johnson and Newman for a simple Helmholtz-like EDL structure [21], and extended decades later by Biesheuvel and Bazant [22] for Gouy-Chapman (GC) EDLs. The latter two models investigated a monoscale porous structure with thin EDLs relative to pore size. In parallel, volume-averaged models were developed for EDLC cells, such as that of Allu *et al.* [23]. More advanced volume-averaged models were later developed to capture effects such as surface transport in EDLs [24,25], and multiscale pore structures with thin EDLs [26]. In addition to mesoscale or macroscale through-electrode pore structure, many CDI and EDLC carbon electrodes include microscale pores with strongly overlapped EDLs for maximized ion storage [27,28]. EDL models used to describe micropore EDLs include modified-Donnan-type [29–31] and amphoteric

(a) E-mail: mesuss@technion.ac.il (corresponding author)

Donnan [32,33]. Beyond carbons, other capacitive electrodes include intercalation sites for ion storage between atomic planes [34–36], where the charged interface is often modeled using Frumkin intercalation isotherms [37,38].

Mathematically, the volume-averaging technique used for capturing charge and ion dynamics in electrochemical systems bears similarity to the Reynold's (time) averaging of mass and momentum conservation equations used to model turbulent fluid flows [39]. While in turbulent flows, the complexity is in time due to random velocity fluctuations induced by eddies [39], in electrochemical systems the complexity is in space due to the random pore structure in typical porous electrodes [40]. One important characteristic of the turbulent flow problem is that time averaging gives rise to a closure problem, as averaging leads to new variables, namely the perturbed flow velocity components. In electrochemical systems, new variables are similarly obtained upon volume averaging, such as the perturbed ion concentration and electric potential. However, in the electrochemical systems literature the closure problem is generally neglected *ad hoc* [21,22,25], for example by assuming "slowly varying parameters" [22], where the perturbed variable's magnitude is assumed to be much smaller than that of the volume-averaged variable.

By contrast, Gabitto and Tsouris posed and solved the closure problem for monoscale capacitively charging porous electrodes with thin Gouy-Chapman-Stern (GCS) EDLs [41]. The latter leveraged the volume-averaging technique pioneered by Whitaker [20], and also applied towards systems such as porous catalysts [42], soil aggregates [43] and biofilms [44]. However, posing and solving the closure problem added significantly more mathematical complexity relative to the simplified volume-averaged model. In this work, we investigate, for a variety of pore shapes and model parameters, under what conditions the closure problem can be neglected with acceptable loss of accuracy. We develop and solve both 2D in-pore models capturing coupled ion and charge dynamics, and the associated 1D volume-averaged models with neglected closure problem in order to carefully compare and evaluate the latter model. Overall, we find that pore shape can have a significant effect on the errors between the in-pore and volume-averaged models, but that in most cases the volume-averaged model gives acceptably accurate results for times significantly longer than the pore diffusion timescale.

Theory. – We here focus on porous media with unimodal pore structure and assume that the pores are filled with an electrolyte containing one univalent anion and one univalent cation with equal diffusivities. In the pore bulk, away from surfaces and so where the electroneutrality condition holds, the balance of salt and charge equations are given as [22,41,45]

$$\frac{\partial \hat{c}}{\partial \hat{t}} = \hat{\nabla}^2 \hat{c}, \tag{1}$$

$$\hat{\nabla} \cdot (\hat{c} \hat{\nabla} \hat{\phi}) = 0, \tag{2}$$

where $\hat{c}$ is the bulk salt concentration ($\hat{c} \equiv \hat{c}_{cation} = \hat{c}_{anion}$), scaled by the initial concentration, c_0, and $\hat{\phi}$ is the bulk electric potential, scaled by the thermal voltage $V_T = kT_e/e$, where k is the Boltzmann constant, T_e is the absolute temperature and e is the elementary charge. Further, $\hat{t}$ is time scaled by the pore diffusion timescale, $\tau_{hp} \equiv h_p^2/D$, where h_p is the pore's characteristic lengthscale, defined by the ratio between the pore's volume and surface area, $h_p \equiv V_p/A_p$, (see fig. A1 in appendix A in the Supplementary Material `Supplementarymaterial.pdf` (SM)), D is the diffusivity and $\hat{\nabla}$ is the Nabla operator scaled by h_p.

We restrict to the case where the EDLs are thin relative to the pore size, h_p, and neglect tangential (surface) transport of ions in the EDLs. Therefore, the boundary condition between the pore surface with an EDL skin and the bulk solution can be described by an effective flux, given as [22,46–48]

$$\hat{\mathbf{n}} \cdot (\hat{\nabla} \hat{c}) = -\varepsilon \frac{\partial \tilde{w}}{\partial \hat{t}}, \tag{3}$$

$$\hat{\mathbf{n}} \cdot (\hat{c} \hat{\nabla} \hat{\phi}) = -\varepsilon \frac{\partial \tilde{q}}{\partial \hat{t}}, \tag{4}$$

where $\hat{\mathbf{n}}$ is the outwards pointing normal vector, ε is the ratio between the Debye length characterizing EDL thickness [49], λ_D, and h_p, and $\tilde{w}$ and $\tilde{q}$ are, respectively, the local areal excess salt and charge densities of the EDL, scaled by $2\lambda_D c_0$. For a GC EDL, the expressions for the EDL excess densities are $\tilde{w} = 4\sqrt{\hat{c}} \sinh^2[(\hat{\phi}_{el} - \hat{\phi})/4]$, and $\tilde{q} = -2\sqrt{\hat{c}} \sinh[(\hat{\phi}_{el} - \hat{\phi})/2]$, where $\hat{\phi}_{el}$ is the electrode potential scaled by the thermal voltage [22,24,25,46].

While eqs. (1) and (2) can be solved together with boundary conditions (3) and (4) for spatiotemporal concentration and potential fields during capacitive charging, the complex geometry of pores in typical porous electrodes can render such an approach difficult. An alternate approach is to develop volume-averaged equations, where the local equations, here eqs. (1) and (2), are integrated over a representative element volume (REV) [50] and re-cast in terms of volume-average parameters (see appendix A in the SM). Such an approach allows for averaging over complexities in pore structure, thus often reducing model dimensionality and enabling simpler boundary conditions. Starting from the local equations (1) and (2), the resulting volume-averaged equations for a general porous structure (eqs. (A15) and (A16) in appendix A in the SM) are given as

$$\frac{\partial(\overline{c_p} + \varepsilon \overline{w_p})}{\partial \overline{t}} + \frac{\overline{c_p}}{p} \frac{\partial p}{\partial \overline{t}} = \frac{1}{p} \overline{\nabla} \cdot (p \overline{\nabla} \overline{c_p}) + \frac{L_e}{h_p \hat{V}_p} \overline{\nabla} \cdot \int_{\hat{A}_p} (\hat{\mathbf{n}} c') \mathrm{d}\hat{A}, \tag{5}$$

$$\varepsilon \frac{\overline{q_p}}{\partial \overline{t}} = \frac{1}{p} \overline{\nabla} \cdot (\overline{c_p} p \overline{\nabla \phi_p}) + \frac{1}{\hat{V}_p} \overline{\nabla} \cdot \int_{\hat{V}_p} c' \overline{\nabla} \phi' \mathrm{d}\hat{V} + \frac{L_e}{h_p \hat{V}_p} \overline{\nabla} \cdot \left[\overline{c_p} \int_{\hat{A}_p} (\hat{\mathbf{n}} \phi') \mathrm{d}\hat{A} \right]. \tag{6}$$

Here $\overline{c_p}$ and $\overline{\phi_p}$ are the dimensionless intrinsic-averaged variables, defined by $\overline{c_p} \equiv \int_{\hat{V}_p} \hat{c}\mathrm{d}\hat{V}/\hat{V}_p$ and $\overline{\phi_p} \equiv \int_{\hat{V}_p} \hat{\phi}\mathrm{d}\hat{V}/\hat{V}_p$, where $\hat{V}_p$ is the pore volume within the REV scaled by h_p^3. There are additionally pore surface area-averaged variables in eqs. (5) and (6), the area-averaged EDL excess salt density, $\overline{w_p} \equiv \int_{\hat{A}_p} \tilde{w}\mathrm{d}\hat{A}/\hat{A}_p$, and excess EDL charge density $\overline{q_p} \equiv \int_{\hat{A}_p} \tilde{q}\mathrm{d}\hat{A}/\hat{A}_p$, where $\hat{A}_p$ represents the pore surface area within the REV scaled by h_p^2. Further, $\overline{t}$ is time scaled by the electrode diffusion timescale, $\tau_{le} \equiv L_e^2/D$, where L_e is the electrode's thickness, $\overline{\nabla}$ is the Nabla operator scaled by L_e and c' and ϕ' are perturbed variables defined by $c' \equiv \hat{c} - \overline{c_p}$ and $\phi' \equiv \hat{\phi} - \overline{\phi_p}$. Finally, p is the electrode's porosity defined by $p \equiv V_p/V_{tot}$, where V_{tot} is the total (solid and liquid phase) volume of the REV.

For the case of homogenous porous media with constant porosity, eqs. (5) and (6) can be simplified to

$$\frac{\partial(\overline{c_p} + \varepsilon\overline{w_p})}{\partial\overline{t}} = \frac{\partial^2\overline{c_p}}{\partial\overline{x}^2} + \frac{L_e}{h_p\hat{V}_p}\overline{\nabla}\cdot\int_{\hat{A}_p}(\hat{\mathbf{n}}c')\mathrm{d}\hat{A}, \tag{7}$$

$$\varepsilon\frac{\overline{q_p}}{\partial\overline{t}} = \frac{\partial}{\partial\overline{x}}\left(\overline{c_p}\frac{\partial\overline{\phi_p}}{\partial\overline{x}}\right) + \frac{1}{\hat{V}_p}\overline{\nabla}\cdot\int_{\hat{V}_p} c'\overline{\nabla}\phi'\mathrm{d}\hat{V} + \frac{L_e}{h_p\hat{V}_p}\overline{\nabla}\cdot\left[\overline{c_p}\int_{\hat{A}_p}(\hat{\mathbf{n}}\phi')\mathrm{d}\hat{A}\right], \tag{8}$$

where $\overline{x}$ is position scaled by L_e. Equations similar to (7) and (8) were presented by Gabitto and Tsouris [41], although there the factor ε multiplying the excess EDL quantities was absent. Equations (7) and (8) contain three terms which include perturbed variables. The right-most terms of eqs. (7) and (8) result from the spatial averaging theorem, as described in previous works [51–53] and in appendix A in the SM. The second term in the right-hand side of eq. (8) results from integrating the nonlinear electromigration term in eq. (2) over the pore volume of the REV (see appendix A in the SM). The latter term bears an analogy to turbulent flows, where the Reynolds stress terms involving velocity perturbations arises from time averaging the nonlinear advection of momentum terms in the Navier-Stokes equation [39]. Overall, both for eqs. (7) and (8), and for the case of turbulent flow, the presence of perturbed parameters suggests the need to pose and solve a closure problem [39,41].

In capacitive charging, the closure problem has typically been neglected *ad hoc* [22,24]. For example, Biesheuvel and Bazant [22] presented and solved the 1D volume-averaged model for capacitive charging of a porous electrode with GC EDLs. The authors rationalized neglecting the closure problem by assuming that the perturbed quantities were small relative to the 1D volume-averaged quantities (so called "slowly varying parameters" on the pore scale). Equations (7) and (8) can then be simplified as

$$\frac{\partial(\overline{c_p} + \varepsilon\overline{w_p})}{\partial\overline{t}} = \frac{\partial}{\partial\overline{x}}\left(\overline{D_{eff}}\frac{\partial\overline{c_p}}{\partial\overline{x}}\right), \tag{9}$$

$$\varepsilon\frac{\partial\overline{q_p}}{\partial\overline{t}} = \frac{\partial}{\partial\overline{x}}\left(\overline{D_{eff}}\,\overline{c_p}\frac{\partial\overline{\phi_p}}{\partial\overline{x}}\right), \tag{10}$$

where here $\overline{D_{eff}} \equiv D_{eff}/D$ represents the scaled effective diffusivity. Dimensional effective diffusivity is defined as $D_{eff} \equiv D/T$, where T is the tortuosity quantifying the increase in diffusion pathways for ions due to the local pore structure. Equations (9) and (10) are identical to the model presented by Biesheuvel and Bazant [22] and by Gabitto and Tsouris [41] and we refer them here as the 1D volume-averaged model.

Another method towards simplifying eqs. (7) and (8) was presented in Gabitto and Tsouris [41]. There, the authors estimated the order of magnitude of the perturbed variables by posing the closure problem. The following two constraints were required:

$$\hat{t} \equiv \frac{tD}{h_p^2} \gg 1, \tag{11}$$

$$\frac{h_p}{L_e} \ll 1. \tag{12}$$

Considering constraints (11) and (12), the perturbed variables behave as [41] $c' = \mathbf{f}_1\cdot\hat{\nabla}\overline{c_p} + f_2\varepsilon\partial\overline{w_p}/\partial\hat{t}$ and $\phi' = \mathbf{f}_1\cdot\hat{\nabla}\overline{\phi_p} + f_2(\varepsilon/\overline{c_p})(\partial\overline{q_p}/\partial\hat{t})$ where $\mathbf{f}_1$ and f_2 are, respectively, vector and scalar functions related to the geometry of the porous structure[1]. Considering the above results, eqs. (7) and (8) become

$$\frac{\partial(\overline{c_p} + \varepsilon\overline{w_p})}{\partial\overline{t}} = \frac{\partial}{\partial\overline{x}}\left(\overline{D_{eff}}\frac{\partial\overline{c_p}}{\partial\overline{x}}\right) + \frac{\partial}{\partial\overline{x}}\left(\varepsilon\frac{\partial\overline{w_p}}{\partial\overline{t}}\frac{h_p}{L_e\hat{V}_p}\int_{\hat{A}_p}\hat{\mathbf{n}}f_2\mathrm{d}\hat{A}\right), \tag{13}$$

$$\varepsilon\frac{\partial\overline{q_p}}{\partial\overline{t}} = \frac{\partial}{\partial\overline{x}}\left(\overline{D_{eff}}\,\overline{c_p}\frac{\partial\overline{\phi_p}}{\partial\overline{x}}\right) + \frac{1}{\hat{V}_p}\overline{\nabla}\cdot\int_{\hat{V}_p} c'\overline{\nabla}\phi'\mathrm{d}\hat{V} + \frac{\partial}{\partial\overline{x}}\left(\varepsilon\frac{\partial\overline{q_p}}{\partial\overline{t}}\frac{h_p}{L_e\hat{V}_p}\int_{\hat{A}_p}\hat{\mathbf{n}}f_2\mathrm{d}\hat{A}\right), \tag{14}$$

where tortuosity was defined as $T \equiv 1/[1 + (\int_{\hat{A}_p}\hat{\mathbf{n}}\cdot\mathbf{f}_1\mathrm{d}\hat{A})/\hat{V}_p]$ [41]. Moreover, the authors argued via a scaling analysis that the right-most term on the right-hand side of eq. (13), and the two right-most terms on the right-hand side of eq. (14) can be neglected, and so eqs. (13) and (14) can be approximated by eqs. (9) and (10) [41].

One additional note is that in past works [22,24,25], the area-averaged variables ($\overline{w_p}$ and $\overline{q_p}$) were assumed

[1] Scaling the problems and their boundary conditions described by eqs. (25)–(30) and (37)–(42) in Gabitto and Tsouris [41] results in identical functions for perturbed concentration and potential.

to be equivalent to the local variables ($\tilde{w}$ and $\tilde{q}$) except with intrinsic volume-averaged quantities replacing local quantities, $\overline{w_p} \approx 4\sqrt{\overline{c_p}}\ \sinh^2[(\hat{\phi}_{el} - \overline{\phi_p})/4]$ and $\overline{q_p} \approx -2\sqrt{\overline{c_p}}\ \sinh[(\hat{\phi}_{el} - \overline{\phi_p})/2]$. The latter assumption was to our knowledge not explicitly justified previously. However, we do so by adapting a technique presented in appendix B in Quintard and Whitaker [54], and find that the expressions for $\overline{w_p}$ and $\overline{q_p}$ used previously are accurate by assuming slowly varying parameters or within the constraints given by eqs. (11) and (12).

Results. – In this work, we evaluate the use of the "slowly varying parameters" assumption invoked to neglect the closure problem and lead to the 1D volume-averaged model of eqs. (9) and (10). To form a basis for comparison, we solved the full, in-pore, 2D model given by eqs. (1) and (2) with pore wall boundary conditions (3) and (4), for several pore shapes. The results of the in-pore model are compared to predictions of the associated volume-averaged model given by eqs. (9) and (10). For all models, the porous separator has a scaled thickness of $\hat{L}_{sep} \equiv L_{sep}/h_p = 10$, and its porosity and tortuosity are equal to those of the electrode. Constant concentration ($\hat{c} = \overline{c_p} = 1$) and potential ($\hat{\phi} = \overline{\phi_p} = 0$) boundary conditions are used at the separator's far end (away from the porous electrode), and zero salt and charge flux conditions are imposed at the electrode's far end (away from the separator). Figures 1(a), (c), and (e) show concentration fields predicted by the in-pore model for a slit-shaped pore at times of $\hat{t} = 0.1$, 1 and 10, respectively. In these figures $\hat{y} = 0$ represents the midline of the pore, the pore wall is at $\hat{y} = 1$, and the interface between the electrode ($\hat{x} \geq 0$) and the separator ($\hat{x} < 0$) is shown schematically by a vertical dashed line. Figures 1(b), (d) and (f) are plots of the predicted concentration profiles from the in-pore model at the pore wall (dotted lines), and from the associated volume-averaged model (solid lines, where $T = 1$ for slit-shaped pore). The parameters used for calculations in fig. 1 include $\hat{L}_e \equiv L_e/h_p = 100$, $\hat{\phi}_{el} = 20$, and $\varepsilon = 0.01$.

In fig. 1(a), we observe that at early times, $\hat{t} = 0.1$, significant perturbation of the bulk electrolyte has occurred near the pore wall at the separator/electrode interface. We also observe strong concentration gradients in both $\hat{x}$ and $\hat{y}$ directions in the latter region, and that elsewhere in the pore the concentration field is largely unperturbed. For the same early time, in fig. 1(b), we observe significant differences between the 2D in-pore model predictions at the wall and that of the 1D volume-averaged model. For example, the minimum dimensionless wall concentration from the 2D in-pore model is 0.84, significantly lower than the minimum concentration of 0.95 predicted by the 1D volume-averaged model. Figure 1(c) shows that at later times where $\hat{t} = 1$, regions of perturbed concentration have diffused to reach the pore midline and into the separator space as well. Also, we observe concentration gradients in both $\hat{x}$ and $\hat{y}$ directions in the pore, with stronger

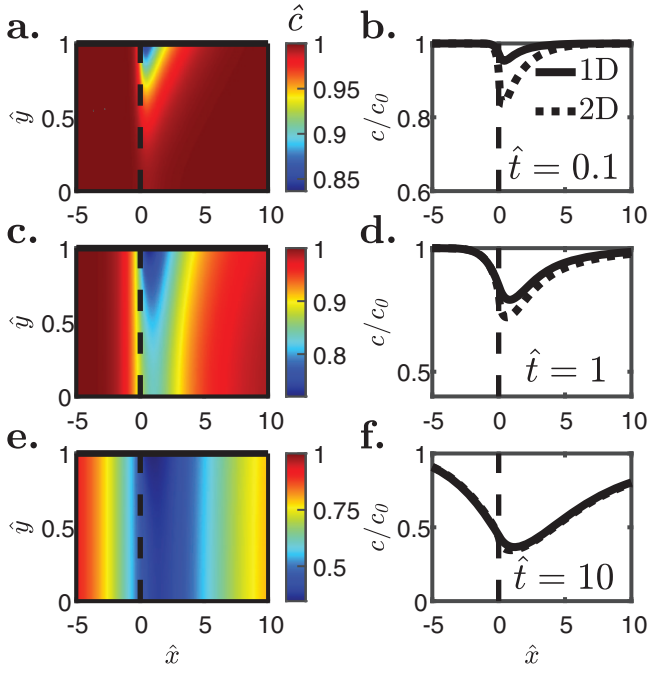

Fig. 1: Predicted concentration fields for the 2D in-pore model ((a), (c) and (e)), and comparisons between the wall concentration of the 2D model to that predicted by the 1D volume-averaged model ((b), (d) and (f)). The times investigated are $\hat{t} = 0.1$ ((a), (b)), $\hat{t} = 1$ ((c), (d)) and $\hat{t} = 10$ ((e), (f)).

gradients in the $\hat{x}$-direction (maximum value of 0.52) compared to the $\hat{y}$-direction (maximum value of 0.37). We also see from fig. 1(d) that at this time, smaller differences are apparent between the 2D and 1D models, as the minimum wall concentration predicted by the 2D model is 0.72, compared to the minimum value of 0.79 predicted by the 1D volume-averaged model. For even later times of $\hat{t} = 10$, we can see in fig. 1(e) the concentration field becomes almost completely one-dimensional in the $\hat{x}$-direction, and likewise fig. 1(f) shows only very slight difference between the concentration profiles of each model, with a minimum of 0.35 predicted by the 2D in-pore model, compared to 0.37 by the 1D volume-averaged model. Thus, from the results of fig. 1, we conclude that for a slit-shaped pore at the aforementioned model parameters, the closure problem can be neglected for times much greater than τ_{hp}, but this simplification can lead to errors at times on the order or smaller than τ_{hp}.

To probe a wider variety of pore shapes, we developed 2D in-pore models and associated 1D volume-averaged models for wavy-walled pores and an idealized pore network. Figures 2(a) to (c) show the pore shaped analyzed, where vertical dashed lines represent the electrode/separator interface and horizontal dot-dashed lines the pores' midlines. Figure 2(a) shows the slit-shaped pore analyzed in fig. 1, where slit-shaped pores with different lengths are analyzed and discussed in appendix C in the SM. For the wavy-walled pores of fig. 2(b), a sinusoidal

function was used to define the wall's location, with wall amplitude of $A = 0.5$, wavelength $\lambda = 2$, both scaled by h_p, and phase angle at the electrode/separator interface of $\theta = 0$. Other pore shapes with varying A, λ, or θ are analyzed and discussed in appendix C in the SM. Figure 2(c) depicts the pore network, characterized by a vertical distance between pores of $\alpha = 1$, and a horizontal distance between pores of $\beta = 0.8$, both scaled by h_p. Other networks with varying α or β are analyzed and discussed in appendix C in the SM. The tortuosity of the wavy-walled pores and pore network was calculated using the definition provided in the "Theory" section, see appendix B in the SM for calculation details. Calculated tortuosity value for the pore shown in fig. 2(b) is 1.23, and 1.27 for that of fig. 2(c). For the 2D model, the parameters for calculations include $\hat{L}_e = 300$, $\hat{\phi}_{el} = 20$ and $\varepsilon = 0.01$. We also plot in figs. 2(a) to (c) the local concentration difference between the 2D and 1D models, $\Delta c \equiv \overline{c_p}(\hat{x}, \hat{t}) - \hat{c}(\hat{x}, \hat{y}, \hat{t})$ scaled by the concentration predicted by 2D model $\hat{c}(\hat{x}, \hat{y}, \hat{t})$, at $\hat{t} = 10$. For the slit-shaped pore (fig. 2(a)), near to the pore inlet, we observe values as high as 0.083 near the walls and as low as -0.082 at the pore midline. For the wavy-walled pore (fig. 2(b)), we see similar trends, where the highest positive value of 0.41 occurs within the apex of the wall sinusoid nearest to the pore inlet. For the pore network (fig. 2(c)), we see values as high as 0.16 near the vertical pores' walls, while values as low as -0.047 develop away from all walls. Overall, at this time, we observe in all pores that the 1D model overpredicts concentration near the walls, and underpredicts near the midline.

In figs. 2(d) and (e), we plot two parameters probing the local and integrated error between the 2D and 1D models. The parameter quantifying local error is $\max|\Delta c/\hat{c}|$, while the integrated error is quantified by $\Delta n_s/\hat{n}_s \equiv (\overline{n}_s - \hat{n}_s)/\hat{n}_s$, where $\hat{n}_s$ is the salt storage predicted by the 2D model, and $\overline{n}_s$ that predicted by the 1D model, both scaled by $2\varepsilon c_0 p V_{el,tot}$, where $V_{el,tot}$ is the total electrode volume. Figure 2(d) shows $\max|\Delta c/\hat{c}|$ as a function of $\hat{t}$, and fig. 2(e) plots $\Delta n_s/\hat{n}_s$ *vs.* $\hat{t}$, both for the slit-shaped pore of fig. 2(a), the wavy-walled pore of fig. 2(b), and the pore network of fig. 2(c). From fig. 2(d), we observe that $\max|\Delta c/\hat{c}|$ evolves differently in time for each pore shape. For example, for the slit-shaped pore (solid black line) a maximum value of 0.14 occurs at $\hat{t} = 0.18$, while the wavy-walled pore (dashed blue line) has a maximum value of 0.41 at the later time of $\hat{t} = 11$. The pore network (dot-dashed red line) reaches a maximum value of 0.24 at even later time of $\hat{t} = 240$. We also notice that only for $\hat{t} > 300$, the value of $\max|\Delta c/\hat{c}|$ decreases for all pore shapes. In contrast to the local error indicator, the integrated error indicator, $\Delta n_s/\hat{n}_s$, in fig. 2(e) shows large values for $\hat{t} < 1$, for example 0.11 at $\hat{t} = 0.03$ for the wavy-walled pore, strongly decreasing as time tends to $\hat{t} = 1$, resulting in good agreement between the models for $\hat{t} > 1$ with highest absolute value of 0.013 for the wavy-walled pore at long times, as expected from constraint (11). Further, we notice the sign of $\Delta n_s/\hat{n}_s$ indicates whether the 2D or 1D model predicts faster charging. For example, the 2D model for the wavy-walled pore is initially slower compared to the associated 1D model, with $\Delta n_s/\hat{n}_s = 0.88$ at $\hat{t} = 0.04$, while for later times the opposite occurs, with $\Delta n_s/\hat{n}_s = -0.011$ at $\hat{t} = 100$.

We can also observe that the curves plotted in fig. 2(d) exhibit a rich variety of non-monotonic features. Such features can occur when the maximum value of Δc changes sign relatively suddenly. For example, for the slit-shaped pore (solid black line), the maximum and minimum scaled differences are, respectively, 0.093 and -0.077 at $\hat{t} = 7$, 0.083 and -0.082 at $\hat{t} = 10$, and 0.076 and -0.084 at $\hat{t} = 13$, resulting in seemingly abrupt changes in the slope at these times in fig. 2(d). Similar phenomena also occur for the wavy-walled pore and the pore network. In appendix C in the SM, we explored a wider range of pore shapes, and find that pore length for a slit-shaped pore does not affect $\max|\Delta c/\hat{c}|$ for $\hat{t} < 1$, but does as time tends to τ_{le}. For example, at $\hat{t} = 100$, $\max|\Delta c/\hat{c}| = 0.13$ for $\hat{L}_e = 30$ ($\overline{t} \approx 0.11$), compared to 0.072 for $\hat{L}_e = 100$ ($\overline{t} = 0.01$) and $\hat{L}_e = 300$ ($\overline{t} \approx 0.0011$). Further, wall amplitude for wavy-walled pores has an important effect on the deviation between the 2D and 1D results, where only for $A > 0.4$ is $\max|\Delta c/\hat{c}|$ well above that of a slit-shaped pore. For the pore network, we observed that increasing α results in higher value of $\max|\Delta c/\hat{c}|$ at $\hat{t} \approx 300$. Overall, while the local error indicator, $\max|\Delta c/\hat{c}|$, can attain relatively large values of over 0.2, even for times longer than τ_{hp}, the integrated error indicator, $\Delta n_s/\hat{n}_s$, is typically of order 0.01 for times much longer than τ_{hp}, consistent with the constraint of eq. (11).

Figures 2(f) to (h) plot various volume-averaged fluxes which underpin terms seen in eq. (14). These fluxes were obtained from the 2D model solution at a time of $\hat{t} = 10$, using an averaging volume of width of $10h_p$. Shown here are results for the slit-shaped pore (fig. 2(f)), the wavy-walled pore (fig. 2(g)) and the pore network (fig. 2(h)). From figs. 2(f) to (h) we see that at $\hat{t} > 1$, electromigration flux due to perturbed fields (red line) is small compared to the corresponding electromigration flux due to averaged fields for all pore shapes (black lines). Small electromigration flux due to perturbed field was also observed for other electrochemical systems not relying on capacitive charging, such as chaotic electroconvection near an ion selective membrane [55,56]. Figure 2(f) shows that the term capturing effects of surface geometry on the EDLs charging process (right-most term of eq. (14)) is uniquely zero, as expected for a pore with unity tortuosity. Figures 2(g) and (h) show noticeable surface geometry effects for a wavy-walled pore and pore network (blue line), although the magnitude of these fluxes is less than that of the electromigration due to averaged fields (black line). Many models for capacitive charging of porous electrodes assume unity pore tortuosity [24,25,57–59], and we here briefly comment on this assumption. When assuming unity tortuosity for pores other than slit-shaped pores,

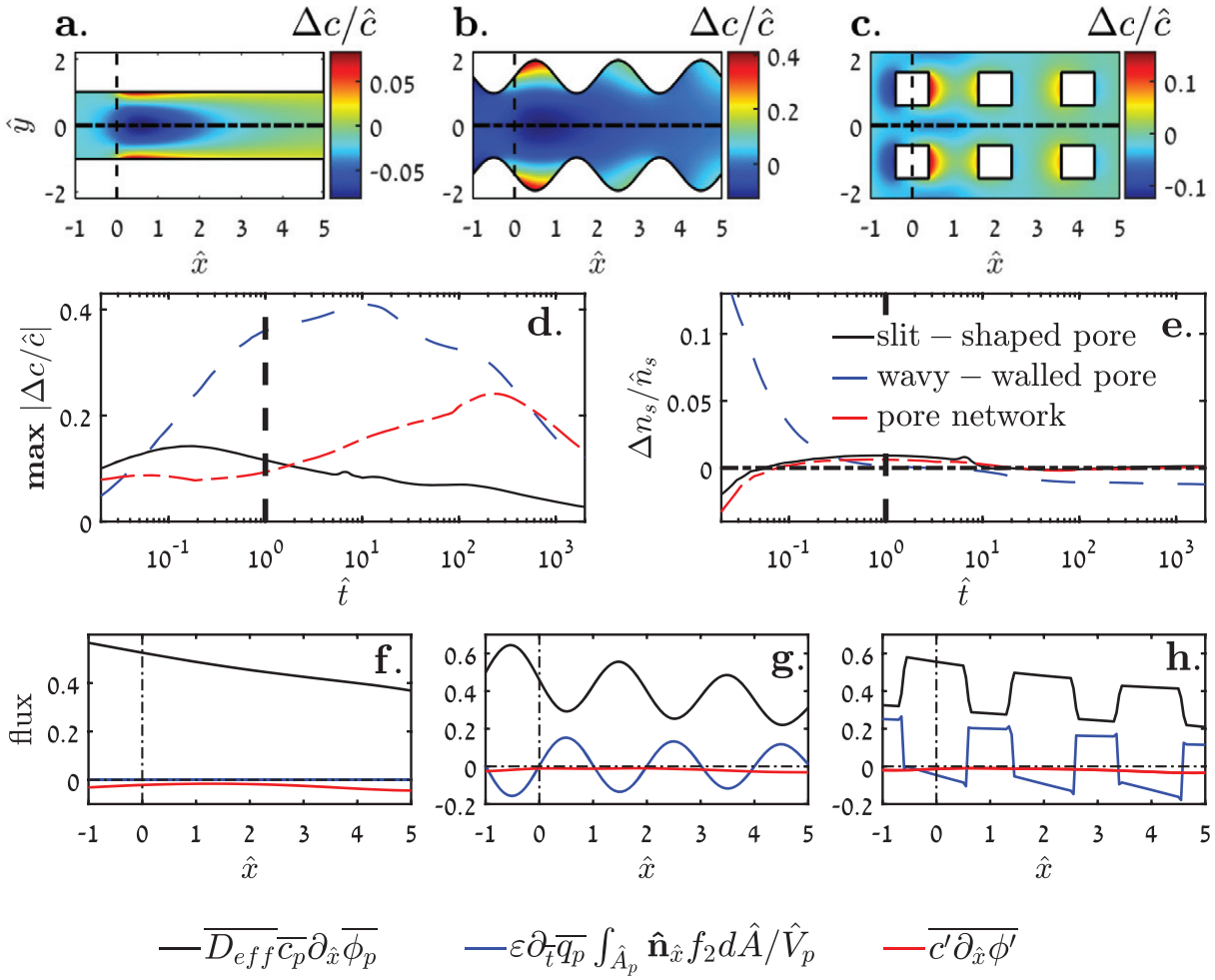

Fig. 2: (a)–(c) Results for the scaled concentration difference between the 2D in-pore model and 1D volume-averaged model, $\Delta c/\hat{c}$, at time $\hat{t} = 10$ for (a) the slit-shaped pore, (b) the wavy-walled pore with $A = 0.5$, and (c) the pore network with $\alpha = 1$ and $\beta = 0.8$. (d), (e): predictions for (d) $\max|\Delta c/\hat{c}|$, and (e) $\Delta n_s/\hat{n}_s$, as a function of $\hat{t}$. (f)–(h) Fluxes involving volume-averaged or perturbed parameters, from eq. (14), at $\hat{t} = 10$, for (f) a slit-shaped pore, (g) a wavy-walled pore with $A = 0.5$ and (h) a pore network with $\alpha = 1$ and $\beta = 0.8$.

$\Delta n_s/\hat{n}_s$ remains large throughout the charging process, decreasing only when nearing steady state. For example, while assuming unity tortuosity for the wavy-walled pore of fig. 2(b), $\Delta n_s/\hat{n}_s = 0.22$ and 0.12 at $\hat{t} = 1$ and $\hat{t} = 10^6$, respectively, compared to 0.0015 and −0.0042 for the same model when accounting for the non-unity tortuosity (fig. C2 in appendix C in the SM), and similar trends were observed for the pore network. Overall, for the pores investigated, the effect of tortuosity is important throughout the charging process, and assuming unity tortuosity may lead to significant errors in predicting the charge and salt dynamics when pores have non-slit shapes.

Conclusions. – We here analyzed the dynamics of capacitive charging of porous electrodes using both 2D in-pore models, and associated 1D volume-averaged models which neglect the closure problem. Long and thin pores of various shapes were analyzed, in order to quantify the error between the in-pore and volume-averaged models. For most pore shapes investigated, neglecting the closure problem resulted in only small deviations in integrated parameters, such as salt stored, between 2D and 1D models at times significantly greater than the pore diffusion time. Local parameters, such as salt concentration, can exhibit more notable deviations, even at times much greater than the pore diffusion time. The approach developed here can be applied to studying multi-scale porous media and a wider variety of pore shapes.

REFERENCES

[1] de Levie R., *Electrochim. Acta*, **8** (1963) 751.
[2] Posey F. A. and Morozumi T., *J. Electrochem. Soc.*, **113** (1966) 176.
[3] Simon P. and Gogotsi Y., *Nat. Mater.*, **7** (2008) 845.
[4] Pandolfo A. G. and Hollenkamp A. F., *J. Power Sources*, **157** (2006) 11.
[5] Miller J. R. and Simon P., *Science*, **321** (2008) 651.
[6] Brogioli D., *Phys. Rev. Lett.*, **103** (2009) 058501.

[7] Rica R. A., Ziano R., Salerno D., Mantegazza F., Van Roij R. and Brogioli D., *Entropy*, **15** (2013) 1388.
[8] Boon N. and van Roij R., *Mol. Phys.*, **109** (2011) 1229.
[9] Suss M. E., Porada S., Sun X., Biesheuvel P. M., Yoon J. and Presser V., *Energy. Environ. Sci.*, **8** (2015) 2296.
[10] Jeon S.-i., Yeo J.-g., Yang S., Choi J. and Kim D. K., *J. Mater. Chem. A*, **2** (2014) 6378.
[11] Seo S. J., Jeon H., Lee J. K., Kim G. Y., Park D., Nojima H., Lee J. and Moon S. H., *Water Res.*, **44** (2010) 2267.
[12] Roelofs S. H., Kim B., Eijkel J. C. T., Han J., van den Berg A. and Odijk M., *Lab Chip*, **15** (2015) 1458.
[13] Zhao R., van Soestbergen M., Rijnaarts H. H. M., van der Wal A., Bazant M. Z. and Biesheuvel P. M., *J. Colloid Interface. Sci.*, **384** (2012) 38.
[14] Porada S., Feng G., Suss M. E. and Presser V., *RSC Adv.*, **6** (2016) 5865.
[15] Mirzadeh M. and Gibou F., *J. Comput. Phys.*, **274** (2014) 633.
[16] Wang G., Mukherjee P. P. and Wang C.-Y., *Electrochim. Acta*, **51** (2006) 3139.
[17] Alizadeh S. and Mani A., *Langmuir*, **33** (2017) 6205.
[18] Alizadeh S. and Mani A., *Langmuir*, **33** (2017) 6220.
[19] Schmuck M. and Bazant M. Z., *SIAM J. Appl. Math.*, **75** (2015) 1369.
[20] Whitaker S., *The Method of Volume Averaging* (Kluwer, Dordrecht) 1999.
[21] Johnson A. M. and Newman J., *J. Electrochem. Soc.*, **118** (1971) 510.
[22] Biesheuvel P. M. and Bazant M. Z., *Phys. Rev. E*, **81** (2010) 031502.
[23] Allu S., Velamur Asokan B., Shelton W. A., Philip B. and Pannala S., *J. Power Sources*, **256** (2014) 369.
[24] Mirzadeh M., Gibou F. and Squires T. M., *Phys. Rev. Lett.*, **113** (2014) 097701.
[25] Shocron A. N. and Suss M. E., *J. Phys.: Condens. Matter*, **29** (2017) 084003.
[26] Gabitto J. and Tsouris C., *Transp. Porous Media*, **113** (2016) 173.
[27] Porada S., Weinstein L., Dash R., van der Wal A., Bryjak M., Gogotsi Y. and Biesheuvel P. M., *ACS Appl. Mater. Int.*, **4** (2012) 1194.
[28] Porada S., Borchardt L., Oschatz M., Bryjak M., Atchison J., Keesman K. J., Kaskel S., Biesheuvel P. M. and Presser V., *Energy Environ. Sci.*, **6** (2013) 3700.
[29] Biesheuvel P. M., Fu Y. and Bazant M. Z., *Phys. Rev. E*, **83** (2011) 061507.
[30] Tang W., Kovalsky P., Cao B. and Waite T. D., *Water Res.*, **99** (2016) 112.
[31] Guyes E. N., Malka T. and Suss M. E., *Environ. Sci. Technol.*, **53** (2019) 8447.
[32] Biesheuvel P. M., arXiv:1509.06354 (2015).
[33] Mubita T., Dykstra J., Biesheuvel P. M., van der Wal A. and Porada S., *Water Res.*, **164** (2019) 114885.
[34] Itaya K., Uchida I. and Neff V. D., *Acc. Chem. Res.*, **19** (1986) 162.
[35] Pasta M., Wessells C. D., Cui Y. and La Mantia F., *Nano Lett.*, **12** (2012) 839.
[36] Shanbhag S., Bootwala Y., Whitacre J. F. and Mauter M. S., *Langmuir*, **33** (2017) 12580.
[37] Levi M. and Aurbach D., *Electrochim. Acta*, **45** (1999) 167.
[38] Singh K., Bouwmeester H. J. M., de Smet L. C. P. M., Bazant M. Z. and Biesheuvel P. M., *Phys. Rev. Appl.*, **9** (2018) 064036.
[39] Launder B. E. and Spalding D. B., *Mathematical Models of Turbulence* (Academic Press, London) 1972.
[40] Newman J. and Thomas-Alyea K. E., *Electrochemical Systems* (J. Wiley) 2004.
[41] Gabitto J. and Tsouris C., *Transp. Porous Media*, **109** (2015) 61.
[42] Jackson R., *Transport in Porous Catalysts* (Elsevier Publishing Co., New York) 1979.
[43] Rappoldt C., *Soil Sci.*, **150** (1990) 645.
[44] Wood B. D. and Whitaker S., *Chem. Eng. Sci.*, **53** (1998) 397.
[45] Guyes E. N., Shocron A. N., Simanovski A., Biesheuvel P. M. and Suss M. E., *Desalination*, **415** (2017) 8.
[46] Bazant M. Z., Thornton K. and Ajdari A., *Phys. Rev. E*, **70** (2004) 021506.
[47] Chu K. T. and Bazant M. Z., *Phys. Rev. E*, **74** (2006) 011501.
[48] Chu K. T. and Bazant M. Z., *J. Colloid Interface Sci.*, **315** (2007) 319.
[49] Russel W. B., Saville D. A. and Schowalter W. R., *Colloidal Dispersions* (Cambridge University Press) 1991.
[50] Bear J., *Modeling Phenomena of Flow and Transport in Porous Media* (Springer International Publishing, Cham) 2018.
[51] Slattery J. C., *AIChE J.*, **13** (1967) 1076.
[52] Anderson T. B. and Jackson R., *Ind. Eng. Chem. Fund.*, **8** (1969) 137.
[53] Whitaker S., *Chem. Eng. Ed.*, **19** (1985) 18.
[54] Quintard M. and Whitaker S., *Adv. Water Resour.*, **22** (1998) 33.
[55] Druzgalski C. L., Andersen M. B. and Mani A., *Phys. Fluids*, **25** (2013) 110804.
[56] Druzgalski C. and Mani A., *Phys Rev. Fluids*, **1** (2016) 073601.
[57] Porada S., Bryjak M., van der Wal A. and Biesheuvel P. M., *Electrochim. Acta*, **75** (2012) 148.
[58] Suss M. E., Biesheuvel P. M., Baumann T. F., Stadermann M. and Santiago J. G., *Environ. Sci. Technol.*, **48** (2014) 2008.
[59] Rubin S., Suss M. E., Biesheuvel P. M. and Bercovici M., *Phys. Rev. Lett.*, **117** (2016) 234502.